Journal of Inflammation Research

Dovepress
open access to scientific and medical research

Open Access Full Text Article

ORIGINAL RESEARCH

Securidaca inappendiculata-Derived Xanthones Protected Joints from Degradation in Male Rats with Collagen-Induced Arthritis by Regulating PPAR-γ Signaling

This article was published in the following Dove Press journal:
Journal of Inflammation Research

Jian Zuo,[1–3,*] Meng-Qing Tao,[1,3,*] Xin-Yue Wu,[4] Tian-Tian Jiang,[1] Opeyemi Joshua Olatunji,[5] Jiyang Dong,[4] Jun Han,[6] Cong-Lan Ji[7]

[1]Department of Traditional Chinese Medicine, The First Affiliated Hospital of Wannan Medical College (Yijishan Hospital), Wuhu, 241000, People's Republic of China; [2]Key Laboratory of Non-coding RNA Transformation Research of Anhui Higher Education Institution, Wannan Medical College, Wuhu, 241000, People's Republic of China; [3]Research Center of Integration of Traditional Chinese and Western Medicine, Wannan Medical College, Wuhu, 241000, People's Republic of China; [4]Department of Electronic Science, Xiamen University, Xiamen, 361005, People's Republic of China; [5]Faculty of Traditional Thai Medicine, Prince of Songkla University, Hat Yai, 90112, Thailand; [6]Drug Research and Development Center, School of Pharmacy, Wannan Medical College, Wuhu, 241000, Anhui, People's Republic of China; [7]School of Pharmacy, Anhui College of Traditional Chinese Medicine, Wuhu, 241000, Anhui, People's Republic of China

*These authors contributed equally to this work

Correspondence: Jun Han
Drug Research and Development Center, School of Pharmacy, Wannan Medical College, Wuhu, 241000, Anhui, People's Republic of China
Email hanjun@wnmc.edu.cn

Cong-Lan Ji
School of Pharmacy, Anhui College of Traditional Chinese Medicine, Wuhu, 241000, Anhui, People's Republic of China
Email 37709103@qq.com

Background: The bark of *Securidaca inappendiculata* Hassk. is traditionally used for treating inflammatory diseases and bone fractures in China. We have previously validated the xanthone-enriched fraction (XRF) of *S. inappendiculata* with anti-rheumatic potentials, but mechanism underlying the joints protective effects is still largely unknown.

Materials and Methods: The male rats with collagen-induced arthritis (CIA) were treated with XRF. The therapeutic efficacy of XRF was evaluated by arthritis score changes, morphological observation of paws, histological examinations and serological analyses. Protein expression in tissues and cells was investigated by either immunohistochemical or immunoblotting methods, while levels of mRNA expression were investigated by RT-qPCR. Metabolites in serum were detected by LC-MS approach. The joints homogenates were used for analyzing possible targeted genes by genome microarray analyses.

Results: Treatment with XRF and methotrexate (MTX) led to significant decrease in arthritis scores, and alleviated deformation of paws in CIA rats. In addition, XRF and MTX reduced circulating TNF-α, IL-1β and IL-17α in the serum and down-regulated TLR4/NF-κB and JNK pathways in joints of CIA rats. Compared to MTX, XRF-loading microemulsion significantly protected joints, which was accompanied by dramatic decrease in MMP3. Differential genes-based KEGG enrichment and metabolomics analysis suggested that XRF reduced fatty acids biosynthesis by regulating PPAR-γ signaling. *S inappendiculata*-derived 1,7-dihydroxy-3,4-dimethoxyxanthone (XAN) up-regulated PPAR-γ expression in macrophages, but suppressed it in pre-adipocytes in vitro, which was synchronized with SIRT1 changes. Adiponectin production and SCD-1 expression in pre-adipocytes were also decreased. Aside the direct inhibition on MMP3 expression in synovioblast, the presence of XAN in macrophages-pre-adipocytes co-culture system further reinforced this effect.

Conclusion: This study revealed the joint protective advantages of the bioactive fraction from *S. inappendiculata* in CIA rats over MTX, and demonstrated that *S. inappendiculata*-derived xanthones suppressed the erosive nature of synovioblast acquired under inflammatory circumstances by regulating PPAR-γ signaling-controlled metabolism-immunity feedback.

Keywords: peroxisome proliferators-activated receptor gamma, PPAR-γ, energy metabolism, rheumatoid arthritis, metabolomics, macrophage, inflammation

Introduction

Securidaca inappendiculata Hassk. is a medicinal plant mainly distributed in southern China. The bark and root of the plant are traditionally used for treating

inflammatory diseases and bone fractures. Pharmacological investigations have confirmed that *S. inappendiculata* possesses impressive therapeutic potentials on rheumatoid arthritis (RA), a common autoimmune disease affecting almost 1% of the global population.[1,2] Although there are many kinds of drugs available for treating RA, such as glucocorticoid, disease-modifying anti-rheumatic drugs (DMARDs) and non-steroidal anti-inflammatory drugs, however successful treatment of RA is still a major challenge in clinical practice due to the complexity of its pathogenesis. Compared to conventional synthetic drugs, herbal medicines have gained prominence in recent years due to their perceived safety profiles and economy merits, and therefore they are extensively used as alternative remedies. Under such contexts, the anti-rheumatic property of *S. inappendiculata* has meaningful clinical implications, and therefore is worthy of further investigations.

In a previous study, we systematically investigated the chemical composition from the back of *S. inappendiculata*, and isolated 11 xanthones as well as several other polyphenols.[3] Subsequently, the xanthone derivatives were identified as the main bioactive components in this plant contributing to the anti-rheumatic property through the regulation of oxidative stress sensitive pathways.[4–6] Furthermore, we confirmed that *S. inappendiculata*-derived xanthones (S-XANs) can directly interact with TLR4, leading to the consequent downregulation of NF-κB and inflammation alleviation.[7] Considering the critical roles of TLR4/NF-κB in innate immunity, these findings are essential for a better understanding of the anti-inflammatory property of *S. inappendiculata*. However, its anti-rheumatic mechanisms are still far away from been well understood. One of the questions to be answered is how *S. inappendiculata* effectively protect joints from damages. As indicated in a previous study, *S. inappendiculata* extract exhibited notable joints protective potentials in rats with collagen-induced arthritis (CIA).[8] This phenomenon cannot be simply interpreted as a piece of evidence for its anti-inflammatory effects. As such, in this present study, we attempted to address this issue using an omics-based strategy. Because herbal medicines are traditionally used in the form of mixtures or extracts, we prepared the xanthone-enriched fraction of *S. inappendiculata* (XRF) for the in vivo pharmacological study. Considering the fact that xanthone derivatives are not readily soluble in water and their oral bioavailability is poor, the XRF-loading microemulsion (XRF-ME) was prepared to improve the clinical performance.[9,10]

Materials and Methods

Chemicals and Reagents

Lyophilized immunization grade bovine type II collagen (CII) and incomplete Freund's adjuvant (IFA) were supplied by Chondex (Redmond, WA). The primary antibodies used for immunoblotting and immunohistochemical assays, including anti- IRF5, MMP3, p-JNK, JNK, p-p65, p65, p-STAT3, STAT3, PPAR-γ, SIRT1, NAMPT, TLR4, GAPDH and β-actin were procured from AB clonal Technology (Wuhan, China). Cell culture reagents, including Dulbecco's Modified Eagle's Medium (DMEM), DMEM/F12 medium, RPMI-1640 medium, fetal bovine serum (FBS), phosphate buffered saline (PBS), trypsin as well as enhanced chemiluminescence detection kit were purchased from Thermo Fisher Scientific (Rockford, IL, USA). HRP/biotin conjugated secondary antibodies, BCA protein quantitation kit, penicillin-streptomycin, protein loading buffer, RIPA lysis buffer together with other chemicals used in the immunoblotting assay were provided by Keygen Biotech (Nanjing, Jiangsu, China). Enhanced sensitivity ELISA kits for TNF-α, IL-1β, and IL-17α determination were purchased from Multi-Science (Hangzhou, Zhejiang, China). TaqMan RT-qPCR kit and cDNA synthesis kit were bought from Solarbio (Beijing, China). Methotrexate (MTX) tablets were commercially available drugs produced by Sine Pharma (Shanghai, China). The solvents/reagents used in LC-MS analysis, including methanol, acetonitrile, ammonium acetate, and ammonium hydroxide were of either spectral or analytical grade and supplied by CNW Technologies (Duesseldorf, German). The selective PPAR-γ inhibitor T0070907 was procured from Selleck Chemicals (Shanghai, China). Ultra-pure water was prepared using a Milli-Q purification system (Millipore, Bedford, MA, USA). The bark of *S. inappendiculata* was obtained from a medicinal herb market in Bozhou, Anhui Province and authenticated by Dr. Jian Zuo, Wannan Medical College. The raw materials were deposited in a controlled indoor environment (temperature < 25°C; relative humidity < 60%) before further experiments, and a voucher specimen (2019-12-008) was kept at Herbarium of Wannan Medical College. The preparation and chemical composition analysis of XRF were performed as detailed in our previous study.[8] In this study, we further demonstrated that xanthone derivatives were

the main components with high abundance in XRF based on a LC-MS analysis with the aid of a natural compounds MS^2 database constructed by Biotree Biotech (Shanghai, China). Main compounds identified were shown in Supplementary S1. 1,7-Dihydroxy-3,4-dimethoxyxanthone (XAN) with the purity of 95% was isolated from *S. inappendiculata* and used as a representative of S-XANs within XRF in the in vitro study.[3]

Preparation of XRF-ME

Systematic optimization of the formula was achieved through an orthogonal test under the guidance of the ternary phase diagram according to our previous report.[10] Isopropyl myristate, Cremophor EL 35 and isopropanol were adopted as the oil phase, surfactant and co-surfactant, respectively. The three solvents were mixed at the ratio of 15:57:28, and additional 2.5% XRF was added on a magnetic stirrer. After the mixture was diluted with the same volume of water, a transparent and homogeneous dispersion was obtained. The transmission electron microscopy observation and droplet distribution analyses revealed that spherical particles within this dispersion system were with a monolayer structure and mean diameter of 24 nm (Supplementary S2). The determination of encapsulation efficiency (EE) was performed as follows: XRF capsulated by microemulsion was eluted from a Sephadex G-50 column, and subsequently quantified by Folin-Ciocalteu method using caffeic acid as a reference standard. EE was calculated based on the ratio of capsulated XRF versus the originally added content. Results from three batches of products showed that the mean EE of XRF-ME was 79.42%. The detailed calculation is included in Supplementary S3.

Induction of CIA in Rats and Treatments

Male Sprague-Dawley rats (7 weeks old) were supplied by Qinglongshan Experimental Animal Company (Nanjing, Jiangsu, China). The animals were housed in separate cages under strictly controlled conditions of temperature (24 ± 2°C) and relative humidity (50 ± 2%) with a 12 h dark/light cycle to simulate the natural rhythm. All the experimental rats had free access to tap water and standard rodent chow. The in vivo experimental procedures were strictly in accordance with the guidelines for the care and use of laboratory animals (United States National Research Council, 2011), and approved by the Ethical Committee of the First Affiliated Hospital of Wannan Medical College (Ethics approval number: YJS 2020-4-014). After 7 days of acclimatization, the rats were administered with a subcutaneous injection of CII-IFA emulsion (2 mg/mL) at the base of the tail, which was followed by another boost subcutaneous injection 7 days after the first injection. After the first subcutaneous injection of CII-IFA, the rats were randomly divided into 5 groups with 6 rats each:

Group 1: Normal healthy control rats

Group 2: CIA control rats

Group 3: CIA rats treated with MTX (in the form of suspension)

Group 4: CIA rats treated with XRF-ME

Group 5: CIA rats treated with XRF suspension (XRF-SU)

The rats in groups 3–5 were treated with either XRF or MTX by oral gavage for 35 days according to the groups they were assigned, while rats in groups 1–2 were given CMC-Na. The treatments started after the first injection of CII-IFA. The preparation of XRF-SU and MTX suspension was as follows: XRF or MTX were firstly dispersed in ethanol, which was then slowly mixed with 0.5% CMC-Na dropwise with continuous stirring. The final content of ethanol in the suspensions was below 2%. To confirm the clinical advantages of XRF-ME, some rats were treated by XRF-SU, and both groups received XRF at 50 mg/kg daily. The rats in MTX group were given 0.33 mg/kg of MTX three times a week.

Therapeutic Effects Evaluation

Throughout the experimental period, the body weight and arthritis scores of rats were periodically recorded using the same criteria described previously.[8] At the end of the in vivo experiment, all the rats were anaesthetized with chloral hydrate. Procoagulant blood samples were collected through abdominal aorta and used for serum preparation. Levels of TNF-α, IL-1β and IL-17α in the serum were determined using the corresponding ELISA kits in accordance with the manufacturer's instructions. After sacrifice, the hind limbs of the animals were dissected from the body and the left ankle joint together with the paw were preserved in 10% buffered formalin for histological examination after decalcification with EDTA solution. Typical histopathological changes including synovial hyperplasia, inflammatory infiltration, angiogenesis and joint degradation were evaluated based on hematoxylin/eosin (H&E) staining. To highlight the protective effects of XRF on cartilage and bone, additional Sarranine O-Fast Green (SOFG) staining was performed. Some other de-waxed

sections were used to evaluate local expression of p-p65 and IRF5 using immunohistochemical method with procedures following a previous report.[8] A portion of the synovium collected from the right knee joint was lysed in RIPA lysis buffer. The expression of MMP3, p-JNK, JNK, p-p65, p65 and TLR4 in heat-denatured samples were assessed by immunoblotting approach using routine procedures. The remaining synovium samples were used in RT-qPCR analyses to determine mRNA expression of gene iNOS, IL-1β, ARG-1, and IL-10. The primer sequences used were included in Supplementary S4.

Genome Microarray Analysis

To identify therapeutic targets of XRF and predict possible joints protective mechanism, samples from CIA and XRF-ME groups were subjected to genome microarray analysis using Agilent Whole Rat Genome Microarray 4×44K chips (Santa Clara, CA, USA). The left knee joints were used in this assay. Attached tissues including skin, muscle and fat were carefully removed. Three samples from each group were mixed, which resulted in two pooled samples for each group. Bone structures together with the intact articular capsule were homogenized in Trizol. Raw RNA extracted was further purified with QIAGEN RNeasy kit according to the manufacture's protocol. cDNA obtained from PCR process was subsequently used as templates for Cy3-tagged cRNA synthesis. Finally, the hybridization process on chips was conducted using the purified cRNA. After extensive washing, the chips were scanned, and obtained images (Supplementary S5) were used for further semi-quantitative analysis.

The raw data was normalized with statistical R package Limma based on the Quantile algorithm. Signals with intensity differences above 2 or below 0.5 between the two groups were taken as differential genes. Subsequently, the pathway enrichment analyses were performed with the aid of R package Bioconductor. Using the online public bioinformatics libraries KEGG (Kyoto Encyclopedia of Genes and Genomes) and GO (Gene Ontology), differential genes were annotated, clustered, and enriched into specific pathways based on their functions and relevance. If over 2 genes from one pathway were significantly regulated by XRF, this signaling was subjected to statistical evaluation by Fisher's test with the built-in tool of clusterProfiler. The predicted target pathways were then ranked according to the statistical assessment using p value as a reference. The top 30 pathways with p value less than 0.05 were deemed as effectively altered.

LC-MS Analysis of Metabolites in the Serum

Prior to the analytical processes, extract solution composed of equal amount of acetonitrile and methanol was prepared, which contained 2 μg/mL of internal standard (IS) L-2-chlorophenylalanine. Firstly, 400 μL extract solution was added to 100 μL of each sample. The mixture was vortex for 30 s, followed by supersonic treatment in ice-water for 5 min. Subsequently, a high-speed centrifugation at 4°C was carried out to precipitate denatured proteins. The supernatant obtained was then dried in a vacuum concentrator, and the resulting residues were dissolved in 50% acetonitrile. Finally, 75 μL of the supernatant obtained upon a further centrifugation (13,000 rpm for 15 min at 4°C) was injected into LC/MS instrument. The quality control (QC) sample was prepared by mixing an equal aliquot of all the analytes, and used to monitor the reliability of the analytical method.

Chromatographic separation was achieved on a ExionLC Infinity UHPLC System (AB Sciex) equipped with a UPLC BEH Amide column (2.1×100 mm, 1.7 μm, Waters). The buffer solution containing ammonium acetate and ammonia hydroxide (25 mmol/L, pH = 9.75) and acetonitrile served as A and B phases, respectively. The gradient elution program was as follows: 0–0.5 min, 95% B; 0.5–7.0 min, 95%-65% B; 7.0–8.0 min, 65%-40% B; 8.0–9.0 min, 40% B; 9.0–9.1 min, 40%-95% B; 9.1–12.0 min, 95% B. The column and auto-sampler temperature were set at 25°C and 4°C, respectively. The separated metabolites were then detected by TripleTOF 5600 mass spectrometry (AB Sciex) with an ESI spray interface under both positive and negative modes, and MS/MS spectra were acquired and processed with Analyst TF 1.7 software. Other analytical conditions adopted were as follows: collision energy, 30 eV; gas 1, 60 psi; gas 2, 60 psi; curtain gas, 35 psi; source temperature, 600°C; decluttering potential, 60 V. Representative total ion chromatograms (TIC) are shown in Supplementary S6.

The TICs obtained were converted to the mzXML format by ProteoWizard, and further processed by a statistical R package XCMS (version 3.2) to filter noise, align signals, and identify common peaks. Because the original intensity of signals varied a lot, the data were initially calculated by comparing with the total area in the chromatograms using IS as a reference, and further normalized using the unit variance scaling (UV) strategy. The processed data were then fed to SIMCA-P V14.1 program

(Umetrics, Umea, Sweden) for principal component analysis (PCA) and orthogonal partial least squares discriminate analysis (OPLS-DA) to overview the metabolic differences between CIA and XRF-ME groups. Afterwards, the metabolites were identified by searching an in-house MS^2 database provided by Biotree Biotech. This database was constructed by combining the public metabolomics database METLIN with spectral data acquired by analyzing over 1400 reference compounds. It covers over 2000 metabolites, mainly organic acids, nucleosides, amino acids, fatty acids, and carbohydrates. Signals sharing MS^2 characteristic similarities over 70% with the references were believed to be reliable and assigned to corresponding compounds.

Cell Culture and Treatments

The rat primary fibroblast-like synoviocytes (FLSs) were graciously provided by Prof. Wei Wei, Anhui Medical University. The pre-adipocytes were prepared in house. Briefly, abdominal fat tissues collected from healthy rats were cut into small pieces, followed by digestion with type I collagenase. After filtering, the unicellular suspension was centrifuged. Cells on the bottom were re-suspended and seeded in culture flasks, and the medium was replaced every 2–3 days. Homogeneous cells obtained after 1 week of culture were taken as pre-adipocytes. To collect peritoneal macrophages, some rats were sacrificed, and 15 mL pre-cooled PBS was injected into the abdominal cavity. The peritoneal exudate fluid was then retrieved with a syringe, and macrophages were harvested after centrifugation at 1000 rpm for 10 min. FLSs, pre-adipocytes and peritoneal macrophages were grown in DMEM, DMEM/F12 and RPMI-1640 medium, respectively, under normal culture conditions (37°C under a humidified atmosphere of 5% CO_2). FLSs and pre-adipocytes from passages 3–6 were used for further experimental procedures, while peritoneal macrophages were used without further passage culture.

FLSs seeded in 6-well plate were pre-stimulated with lipopolysaccharide (LPS) for 1 h, and then treated with XAN at various concentrations (2.5, 5 and 10 μg/mL). After 12 hours of incubation, the cells were collected and lysed. Expression of MMP3 as well as proteins involved in its regulation including p-JNK/JNK, p-STAT3/STAT3, NAMPT/SIRT1 was assessed by immunoblotting method. To mimic the inflammatory immune microenvironment in joints and decipher the clinical implications from metabolic regulation by XRF, pre-adipocytes and macrophages were co-cultured in transwell (with pores of 0.4 μm, allowing XAN and cytokines to permeate), and subsequently stimulated with LPS in combination with XAN. Briefly, pre-adipocytes (1×10^6 per well) were allowed to attach to the lower chamber, while peritoneal macrophages were seeded onto the upper chamber. These cells were then pre-stimulated with LPS (400 ng/mL) for 1 h, followed by further XAN treatment for 12 h. Adiponectin within the medium was quantified using the ELISA kit provided by Multi-Science (Hangzhou, Zhejiang, China). The supernatant obtained was mixed with equal amount of fresh medium, and subsequently used for FLSs culture, which lasted for an additional 6 h. Finally, all the cells including FLSs, pre-adipocytes and macrophages were harvested for PCR and immunoblotting analyses. To evaluate the net effects brought by the co-culture system, mono-cultured cells with or without LPS pre-treatment were used as controls. Primer sequences for β-actin, MMP3, SCD-1, SIRT1 and PPAR-γ were listed in Supplementary S4. To verify the up-regulatory effects of XAN on PPAR-γ signaling in macrophages and investigate the immune consequences, some LPS-primed cells were treated with XAN (5 μg/mL) in the combination with T0070907 (a selective PPAR-γ inhibitor) for 12 h, and levels of PPAR-γ, iNOS, ARG-1, IL-1β, IL-10 were determined by RT-qPCR method.

Statistical Analysis

Quantification data were presented as mean ± standard deviation. Statistical differences among groups were analyzed by GraphPad Prism 8.0 (GraphPad Software, Cary, NC) using one-way analysis of variance coupled with Tukey post hoc test. P values <0.05 or 0.01 were considered statistically significant.

Results

ME System Improved the Anti-Rheumatic Potentials of XRF

The administration of *S. inappendiculata*-derived xanthones at a maximum dose of 100 mg/kg did not lead to obvious toxicity in mice.[4] In addition, the long-term treatment with XRF at 80 mg/kg was also confirmed to be safe in rats.[8] Consistent to these observations, XRF in the forms of either XRF-SU or XRF-ME at 50 mg/mL did not cause any abnormal reactions in the tested animals in this study.

The therapeutic effects of XRF on CIA have been previously investigated.[8] In this study, we further highlighted the therapeutic advantages of XRF-ME over XRF-SU. The spontaneous CIA remission occurs approximately 30 days after the first immunization, and the increase in pro-inflammatory cytokines as well as the inflammatory manifestation is hard to be observed during the later stages. Therefore, the experimental duration was designated as 28 days after the boost subcutaneous injection. As shown in Figure 1A, the body weight gain in CIA rats was constantly and significantly less than the healthy normal control rats, whereas, the administration of MTX and XRF-SU effectively restored the body weight in CIA rats. However, there was no difference between CIA controls and XRF-ME treated rats. Although the overall therapeutic efficacy of XRF seems to be weaker than MTX, XRF-ME treatment also achieved significant decrease in arthritis score. All the pro-inflammatory cytokines tested namely TNF-α, IL-1β and IL-17α were significantly reduced by both XRF-ME and MTX treatments, while XRF-SU exhibited the weakest effect (Figure 1B). Accordingly, obvious morphological recovery of hind paws was achieved upon XRF-ME and MTX treatments, while the bulbous swelling and joints deformation can be still noticed in XRF-SU-treated rats (Figure 1C). Arthritis-related histological changes were ameliorated too. Comparatively, the joints protective effects of XRF were even better than MTX, as demonstrated by the intact cartilage from XRF-ME-treated rats (Figure 1D). These evidences suggested that ME delivery system maximized the bioactivity of XRF in vivo as anticipated. As such, the subsequent mechanism investigation was mainly conducted on XRF-ME treated rats.

XRF Altered Macrophage Polarization in Joints of CIA Rats

H&E staining-based histological observation preliminarily revealed the effective joints protective effects of XRF-ME. To confirm these findings, we specifically stained cartilages and bones with SOFG. Intact subchondral structures were observed in healthy control rats, which were covered with a continuous layer of cartilage, while the structures in CIA rats were totally disordered (Figure 2A). Extensive degradation and abnormal bone/cartilage fusion were observed in CIA control rats, and these pathological changes were reflected in joints ankylosis. Although MTX alleviated the joint space narrowing, it barely improved bone/cartilage erosion. Whereas, treatment with XRF-ME resulted in significant improvement of joints damages, irrespective of the fact that its effect on pro-inflammatory cytokines increase was not as efficient as MTX.

As pro-inflammatory macrophages are believed to activate FLSs and initiate tissue degradation in joints, we investigated the expression of p-p65 and IRF5 in the synovium, two important indicators of M1 polarization.[11] Increased expression of p-p65 and IRF5 was observed in the CIA control rats, which served as a solid evidence for NF-κB activation and unbalanced macrophages polarization (Figure 2A). Unsurprisingly, as a first-line DMARD, MTX effectively contained these changes, and so did XRF-ME. Furthermore, we investigated the protein expression of p-JNK, JNK, p-p65, p65, MMP3 and TLR4 in the synovium with the immunoblotting method. Similar to results from immunohistochemical assay, both MTX and XRF-ME inhibited the phosphorylation of JNK and p65, and reduced TLR4 expression (Figure 2B). More blot images obtained from this assay were included in Supplementary S7. Interestingly, significant decrease in MMP3 (a direct executor of joints degradation) occurred only under XRF-ME treatment, which further convinced us that *S. inappendiculata* was more effective in protecting joints than MTX (Figure 2C). The effects of treatments on macrophages were further validated by RT-qPCR analyses performed on synovium. Similar to MTX, XRF-ME was favorable for the expression of mRNA ARG-1 and IL-10. Contrarily, it inhibited iNOS and IL-1β expression (Figure 2D). As XRF showed no advantage over MTX concerning the effects on macrophage polarization, it suggested that the profound decrease in MMP3 expression under XRF-ME treatment could be mediated by FLSs, another key player accounting for joints degradation in RA.[12] Besides, these observations suggested the different therapeutic mechanisms of MTX and XRF on RA/CIA, a hypothesis supported by our recent study.[13] MTX suppresses several classic pro-inflammatory pathways in immune cells by activating adenosine receptors.[14] Therefore, XRF could induce MMP3 decrease in CIA rats through a mechanism that is largely independent from JNK and NF-κB pathways.

PPAR Pathways Regulation Involved in Therapeutic Actions of XRF on CIA Rats

A total of 735 differential genes were screened out upon comparison between CIA and XRF-ME groups based on results from genome microarray analysis. The following

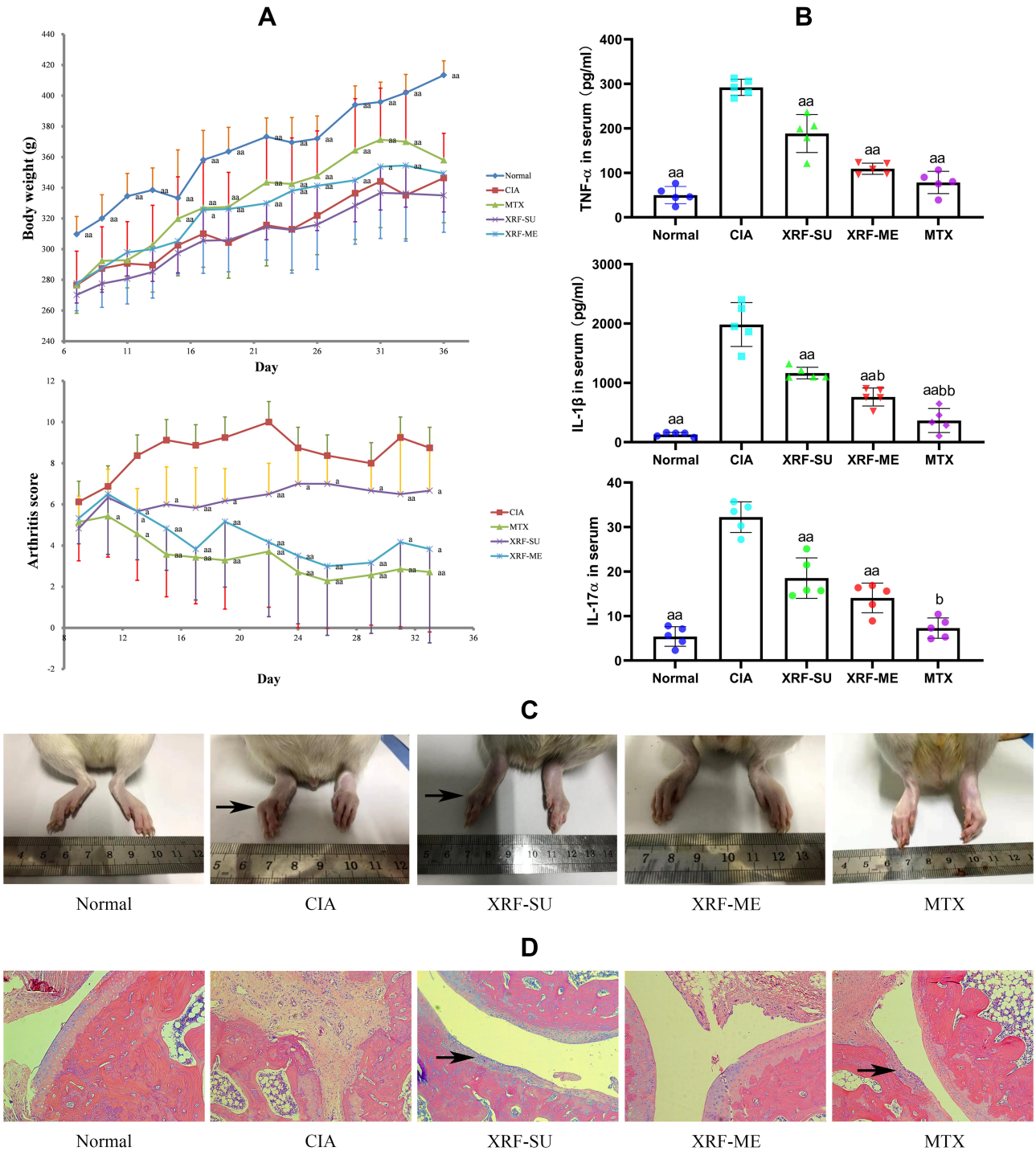

Figure 1 Therapeutic effects of XRF and MTX on CIA rats. (**A**) Body weight and arthritis score changes in rats during the experimental period; (**B**) levels of serological biomarkers evaluated by ELISA method; (**C**) morphology observation of the inflamed hind paws (black arrow: bulbous swelling and joints deformation); (**D**) histological examination of ankle joints (H&E staining, black arrow: cartilage erosion and inflammatory infiltration). The data were presented as mean ± standard deviation. Results were statistically analyzed using one-way ANOVA followed by Tukey post hoc test. Statistical significance: $^{a}p < 0.05$ and $^{aa}p < 0.01$ compared with CIA models, $^{b}p < 0.05$ and $^{bb}p < 0.01$ compared with XRF-SU treated rats.

Abbreviations: CIA, collagen-induced arthritis; XRF, xanthone-enriched fractions of *S. inappendiculata*; XRF-ME, XRF loading microemulsion; XRF-SU, XRF suspension; H&E, Hematoxylin/Eosin.

GO enrichment indicated that XRF treatment had profound impacts on extracellular matrix (ECM) biosynthesis (Figure 3A). Some representative ECM genes altered by XRF-ME in CIA rats were displayed in the form of heatmap in Figure 3B. Most of them belong to the collagen family, which is indispensable for bone remodeling. It is

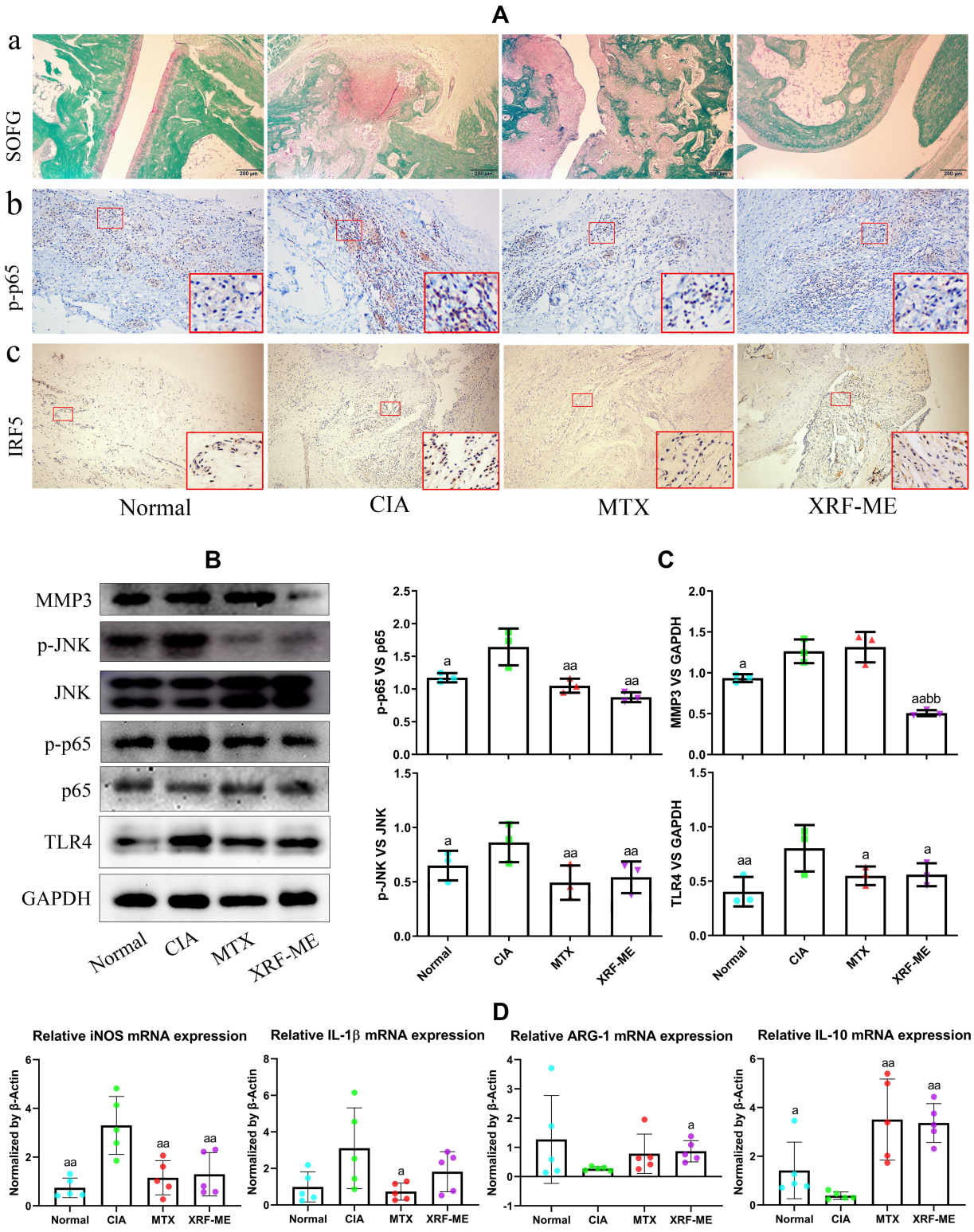

Figure 2 Effects of treatments on tissue damages and inflammatory pathways in joints in CIA rats. (**A**) a, histological examination of joints structures (SOFG staining, cartilages and bones were stained by pink and green, respectively), b-c, immunohistochemical examination of p-p65 and IRF5 expression in synovium; (**B**) expression of protein MMP3, TLR4, p-p65/p65, p-JNK/JNK in synovium investigated by immunoblotting method; (**C**) quantification results of assay (**B**); (**D**) expression of mRNA iNOS, IL-1β, ARG-1, IL-10 in synovium determined by RT-qPCR method. The data were presented as mean ± standard deviation. Results were statistically analyzed using one-way ANOVA followed by Tukey post hoc test. Statistical significance: $^{a}p < 0.05$ and $^{aa}p < 0.01$ compared with CIA models, $^{bb}p < 0.01$ compared with MTX treated rats.
Abbreviation: SOFG, Sarranine O-Fast Green.

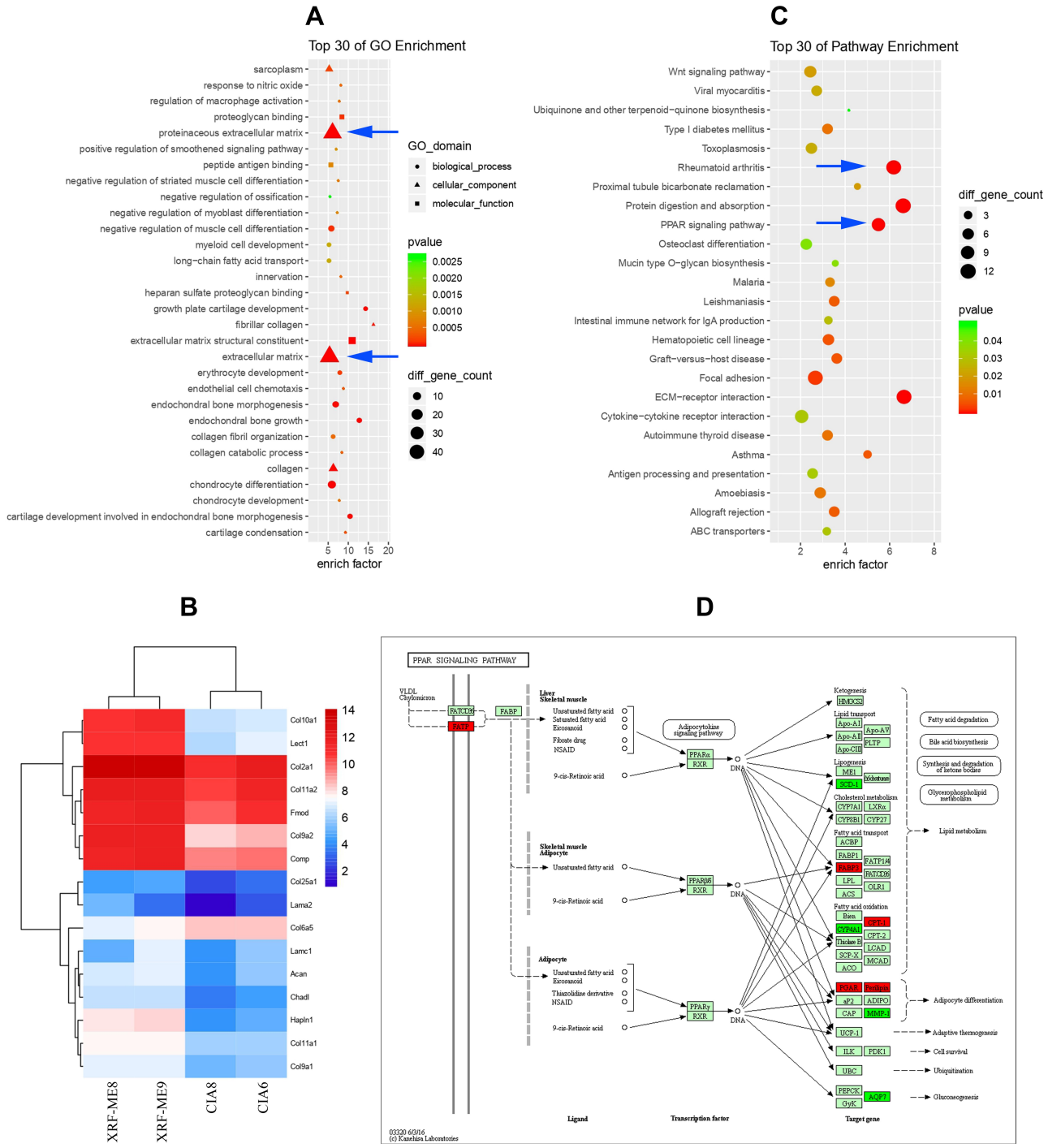

Figure 3 Results of genome microarray analysis. (**A**) GO pathway enrichment based on differential genes between CIA and XRF-ME groups (blue arrow: proteinaceous extracellular matrix and ECM pathways); (**B**) expression levels of representative ECM genes in the two groups; (**C**) KEGG pathway enrichment (blue arrow: rheumatoid arthritis and RRAR signaling pathways); (**D**) PPAR signaling-related genes regulated by XRF (annotated by KEGG, green: down-regulated, red: up-regulated).
Abbreviations: ECM, extracellular matrix; GO, gene ontology; KEGG, Kyoto Encyclopedia of Genes and Genomes.

highly plausible that XRF relieved joint degradation by up-regulating collagen and other bone ECM production. KEGG enrichment analysis showed that aside from RA and ECM-receptor pathways, PPAR signaling was the most significantly altered upon treatment with XRF-ME (Figure 3C). Since PPARs especially PPAR-γ are deeply involved in metabolism and immune regulations, these findings suggest a unique anti-rheumatic mechanism of XRF.[15] It should be specifically noted that XRF exerted a totally different effect on the downstream targets.

SCD-1, MMP-1, AQP7, and CYP4A1 were down-regulated by XRF, while FABP3, CPT-1, PGAR, and Penlipin were up-regulated (Figure 3D).

XRF Altered Lipid Metabolism in CIA Rats Based on LC-MS Analysis of Serum

It is widely accepted that PPARs govern lipid metabolism.[15] Therefore, we analyzed metabolites in the serum of XRF-treated CIA rats using the LC-MS approach to find out if XRF altered lipid metabolism in CIA rats. The metabolites-based PCA indicated that XRF-ME and CIA groups were distinctly differentiated. Meanwhile, the plots of QC sample totally overlapped in the scatter diagram. It suggested the robustness of the analytical method, and the altered metabolic profile of CIA rats under XRF-ME treatment. OPLS-DA validated by permutation test confirmed the effects of XRF on lipid metabolism in CIA rats (Figure 4A). Among the identified metabolites, 73 and 59 signals ($p < 0.05$, VIP > 1) from the negative and positive detection modes were screened out as statistically different between the two groups, which were then subjected to further clustering analysis. Samples from the same group were clustered correctly using the data obtained from either negative or positive mode, suggesting the differentiating potentials of these metabolites (Figure 4B). It was noticed that majority of these differential metabolites belong to lipids and small peptides. Thereafter, we displayed them separately in Figure 4C based on categories. All free fatty acids (FFAs) determined were significantly reduced by XRF, as well as lipoids, such as phosphatidylethanolamine (PE) and phosphatidylcholine (PC) derivatives. It has been confirmed that saturated FFAs promote inflammation by activating TLR4 signaling.[16] Reduced octadecanoic acid under XRF-ME treatment may have contributed to the eased inflammation in CIA rats. More importantly, it suggested that XRF inhibited adipogenesis in vivo, by taking its negative effects on circulating malonyl-CoA and adipocytes size into consideration.[8] Accelerated PC turnover was found to correlate with inflammation in adipose tissues.[17] Thus, the reduced LysoPC (22:6 (4Z,7Z,10Z,13Z,16Z,19Z)), LysoPC (16:0) and PC (O-14:1 (1E)/0:0) observed under XRF-ME treatment seems to be favorable in controlling chronic inflammation and obesity-related symptoms. All these clues suggested that XRF could improve inflammation in CIA rats by suppressing lipid anabolism, considering the fact that RA patients usually develop hyperlipemia and central obesity.[18] The effects of XRF on peptides were diversified, and we categorized the altered peptides based on their relevance to CII, a major ingredient in the cartilage. It is well known that CII composition is rich in glycine and proline but lacks tryptophan.[19] It is interesting to observe that all peptides comprising either proline or glycine were reduced by XRF. Other peptides especially those containing tryptophan were largely increased. Three out of the seven increased peptides detected in this study contained tryptophan residue. It suggested that XRF selectively prevented CII from degradation in CIA rats.

FLS Was Not the Direct Target of XRF Involving PPAR-γ Regulation

FFAs biosynthesis is selectively controlled by PPAR-γ rather than other members from this family, the results from LC-MS analysis indicated the possible effects of XRF on PPAR-γ.[15] Since PPAR-γ is rigorously controlled by SIRT1, we investigated the expression of PPAR-γ and SIRT1 in the synovium of rats.[20] XRF obviously increased PPAR-γ expression compared to MTX. SIRT1 was suppressed by both XRF and MTX (Figure 5A). It further proved that XRF was capable of activating PPAR-γ signaling, as SIRT1 and PPAR-γ have reciprocal negative effects on each other's expression.[20] As deduced above, FLSs rather than macrophages could be the major therapeutic target of XRF accounting for its joints protective potentials. Thereafter, we investigated the effects of XAN on FLSs in vitro to observe its possible regulatory effects on PPAR-γ signaling. To mimic the inflammatory conditions, we pre-treated normal FLSs with LPS, as they express TLR4. However, PPAR-γ expression was too low to be detected by the immunoblotting method due to the selective distribution of PPAR-γ.[21] Levels of MMP3 as well as its upstream signals were reduced by XAN, but only at high concentrations (above 5 μg/mL) (Figure 5B). Although both MTX and XRF inhibited the expression of NAMPT, its downstream SIRT1 was barely affected (Figure 5C). Consequently, the possibility of the joints protective effects resulting from FLSs-related PPAR-γ regulation under XRF treatments was basically ruled out due to the low expression of PPAR-γ. Additionally, many studies have confirmed the poor oral bioavailability of xanthones.[22] Delivery of these constituents into joints was even more difficult.[10] It implied that the reduced

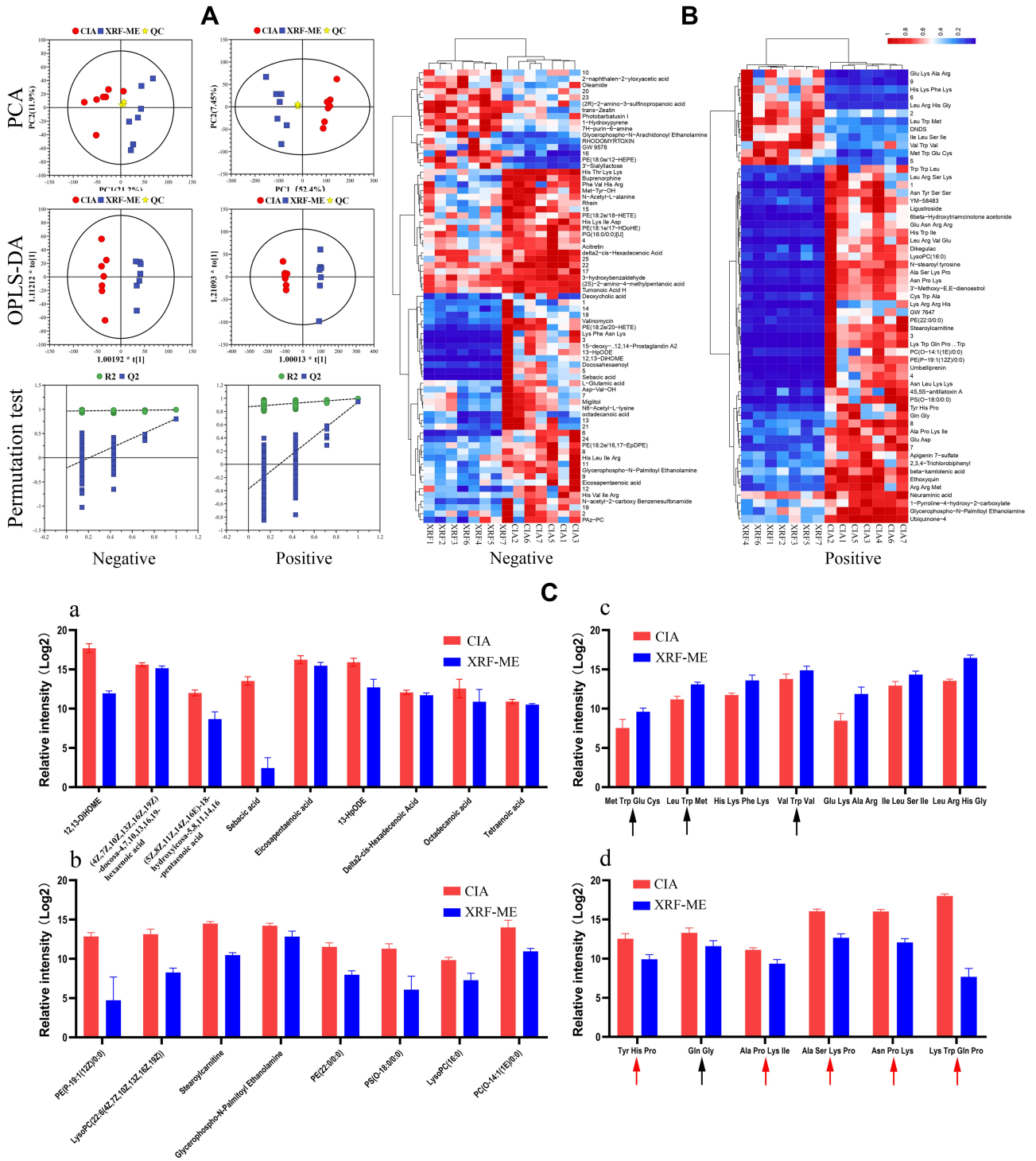

Figure 4 LC-MS analysis of metabolites in serum. (**A**) Overview of the metabolic profile difference between CIA and XRF-ME groups based on PCA and OPLS-DA analyses; (**B**) heatmap of differential metabolites detected under both negative and positive ion modes; (**C**) representative metabolites displayed by categories: a, FFAs, b, lipoids, c, small peptides increased by XRF (black arrow: peptides containing tryptophan), d, small peptides decreased by XRF (black arrow: peptides containing glycine; red arrow: peptides containing proline).

Abbreviations: FFAs, free fatty acids; PCA, component analysis; OPLS-DA, orthogonal partial least squares discriminate analysis.

joints damages observed upon XRF-ME treatment could be attributed to improvement of immune microenvironment rather than directly targeting FLSs. That is, XRF could regulate PPAR-γ signaling in peripheral cells, and consequently improved the pro-inflammatory immune milieu required by FLSs to maintain the erosive properties.

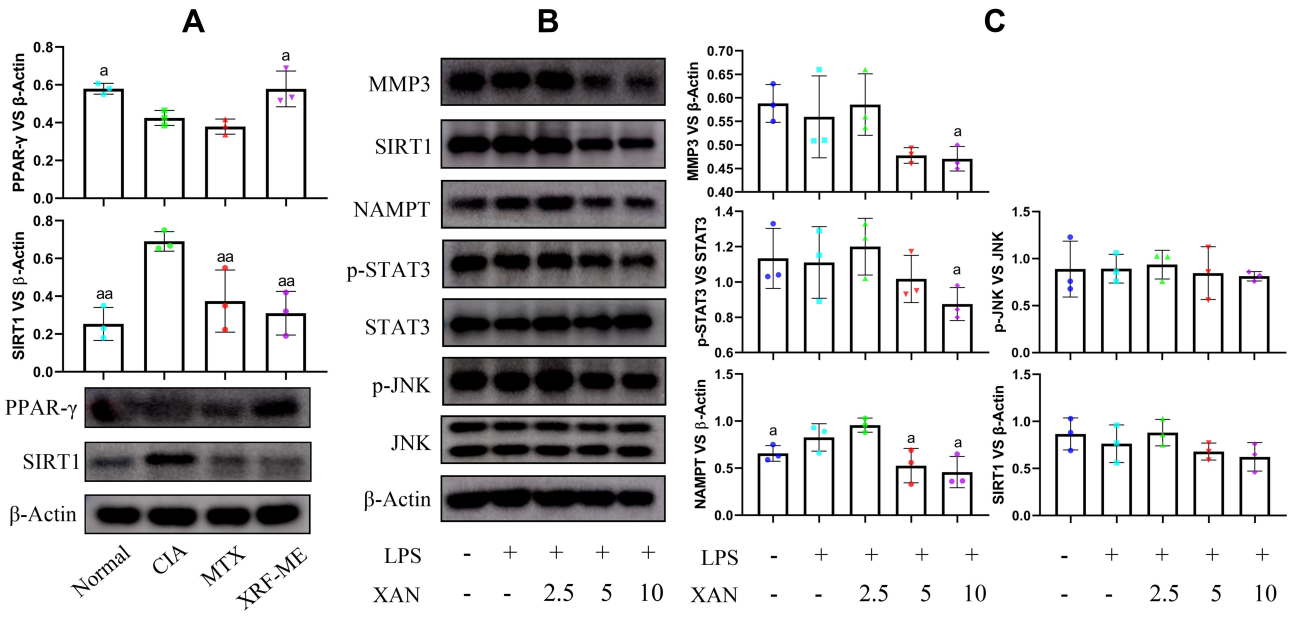

Figure 5 Immunoblotting analysis of synovium from CIA rats and FLSs treated by XAN. (**A**) Expression of PPAR-γ and SIRT1 in synovium from CIA rats receiving different treatments; (**B**) expression of protein MMP3, SIRT1, NAMPT, p-STAT3/STAT3 and p-JNK/JNK in FLSs receiving XAN treatments in the presence of LPS; (**C**) quantification results of image (**B**). Unit for the concentration in assay (**B**) was μg/mL. The data were presented as mean ± standard deviation. Results were statistically analyzed using one-way ANOVA followed by Tukey post hoc test. Statistical significance: image (**A**), $^{a}p < 0.05$ and $^{aa}p < 0.05$ compared with CIA control, image (**C**), $^{a}p < 0.05$ compared with LPS-treated cells.

Abbreviations: XAN, 1,7-dihydroxy-3,4-dimethoxyxanthone; FLSs, fibroblast-like synoviocytes; LPS, lipopolysaccharide.

XRF Improved the Immune Milieu by Regulating PPAR-γ Signaling

Given the fact that PPAR-γ is widely expressed in myeloid cells, namely macrophages in the case of flamed joints under RA conditions, we assumed that XRF mainly regulated PPAR-γ in macrophages in the joints. Meanwhile, PPAR-γ is highly expressed by pre-adipocytes, which plays a central role in fat metabolism homeostasis and extensively interacts with macrophages under inflammatory circumstances.[23] Considering their reciprocal interactions and the significant immune significance, we treated macrophages and pre-adipocytes with XAN in the presence of LPS in a co-culture system. It was very obvious that the stimulus of LPS on both cells was exaggerated in the case of co-culture. Interestingly, the overall effects of XAN on macrophages and pre-adipocytes were totally different. XAN decreased PPAR-γ and increased SIRT1 in pre-adipocytes, but the opposite effects were observed in macrophages (Figure 6A). Because PPAR-γ promotes M2 polarization in macrophages, XAN-elicited up-regulation of this signaling could contribute to the eased inflammation.[21] As anticipated, the changes in the expression of mRNA iNOS, ARG-1, IL-1β and IL-10 induced by LPS were restored by XAN, while these effects were greatly antagonized by the selective PPAR-γ inhibitor T0070907 (Figure 6B). It basically confirmed that XAN can improve the immune microenvironment by activating PPAR-γ signaling in macrophages either in vivo or in the co-culture system. To figure out the net impact on joints from the interplay between macrophages and pre-adipocytes and XAN-elicited influences, we cultured FLSs with the medium collected from the co-culture system. Majority of XAN had been catabolized and eliminated during the co-culture process, and the remaining XAN content was too low to be determined by UPLC-UV (Supplementary S8). As such, it largely ruled out the interference from direct XAN stimulus. RT-qPCR analysis indicated a dramatic increase in MMP3 expression induced by the medium collected from inflammatory conditions, while the presence of XAN in the co-culture system effectively abolished this trend (Figure 6C). Immunoblotting assay showed that not only MMP3 but also its upstream STAT3 in FLSs were down-regulated by XAN (Figure 6D and E). We subsequently focused on changes of pre-adipocytes in the co-culture system. As illustrated in Figure 6F, synthesis of adiponectin, a representative adipokine was promoted by LPS-primed macrophages, while the co-existence of XAN significantly reduced it. RT-qPCR analysis indicated that XAN down-regulated SCD-1, the downstream of PPAR-γ and also a key regulator in FFAs

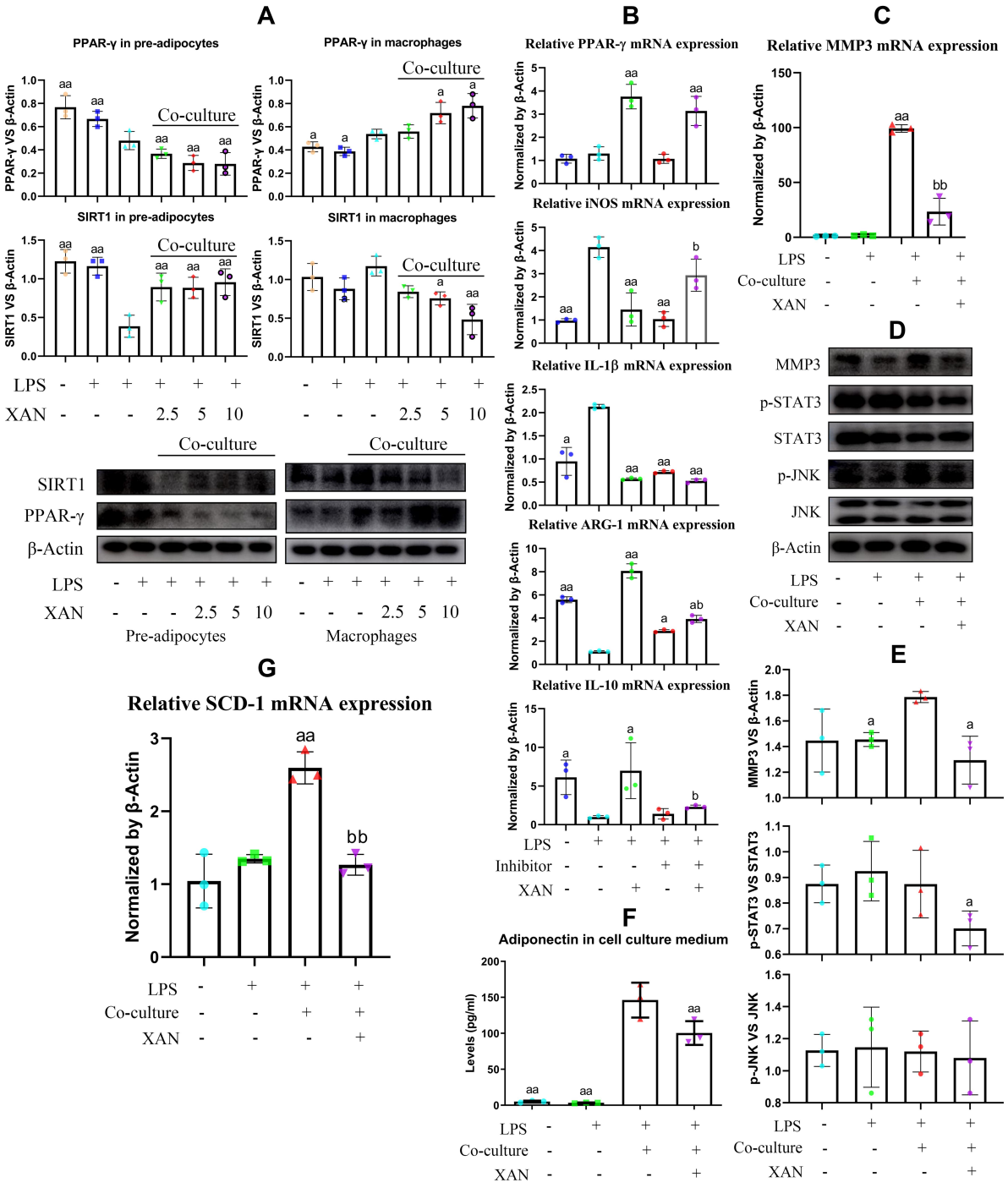

Figure 6 Regulation of XAN on PPAR-γ signaling in co-cultured pre-adipocytes and macrophages in vitro and its influence on FLSs. (**A**) Expression of SIRT1 and PPAR-γ in pre-adipocytes and macrophages from either mono-culture or co-culture systems under the stimulus of XAN in combination of LPS, investigated by immunoblotting method; (**B**) effects of the selective PPAR-γ inhibitor T0070907 on XAN-induced expression changes of mRNA PPAR-γ, iNOS, ARG-1, IL-1β, IL-10 in macrophages, investigated by RT-qPCR method; (**C**) expression of mRNA MMP3 in FLSs treated by LPS or cultured with medium collected from pre-adipocytes-macrophages co-culture system in the presence of LPS or together with XAN, investigated by RT-qPCR; (**D**) expression of protein MMP3, p-STAT3/STAT3, p-JNK/JNK in FLSs receiving the same treatments as assay (**C**), investigated by immunoblotting method; (**E**) qualification results of assay (**D**); (**F**) adiponectin released by pre-adipocytes in the co-culture system in the presence of LPS or together with XAN, investigated by ELISA method; (**G**) expression of gene SIRT1, SCD-1 and PPAR-γ in pre-adipocytes obtained from assay (**F**), investigated by RT-qPCR. Unit for the concentration of XAN in assay (**A**) was μg/mL; the concentration of XAN adopted in assay (**B**–**G**) was 5 μg/mL. The data were presented as mean ± standard deviation. Results were statistically analyzed using one-way ANOVA followed by Tukey post hoc test. Statistical significance: image (**A** and **B**), $^{a}p < 0.05$ and $^{aa}p < 0.01$ compared with LPS-treated cells, $^{b}p < 0.05$ compared with XAN+LPS-treated cells; image (**E**–**G**), $^{a}p < 0.05$ and $^{aa}p < 0.01$ compared with LPS-treated cells from co-culture system, $^{bb}p < 0.01$ compared with LPS+XAN-treated cells from co-culture system.

biosynthesis (Figure 6G). Generally, it demonstrated that by regulating PPAR-γ, XAN intervened into adipogenesis. Different outcomes observed on macrophages and pre-adipocytes under XAN stimulus also provided evidence explaining the diversified effects of XRF on the downstream targets of PPARs signaling.

Discussion

Imbalanced ratios in Th17/Treg as well as Th1/Th2 cells were found to be restored under xanthones treatment.[24,25] Because RA is deemed as a $CD4^+$ lymphocytes-driven disease, these findings solidly confirmed their anti-rheumatic potentials. Many theories have been proposed to explain their effects on adaptive immunity, and the monocytes/macrophages-mediated mechanism seems to be comparatively convincing.[25] Manipulating either the population or polarization of macrophages are both feasible approaches to disrupt the abnormal activation of adaptive immunity under pathological conditions. We noticed that XAN had no obvious cytotoxicity on macrophages in vitro at concentrations below 10 μg/mL.[7] Considering the low distribution of xanthones after oral administration, it suggested that XAN alleviated macrophages-controlled inflammation through a manner other than cytotoxicity. The potent inhibitory effects of α-mangostin at non-toxic concentrations on NF-κB pathway preliminarily supported this claim.[26] Subsequently, the direct interaction between XAN and TLR4 was identified.[7] As TLR4/NF-κB activation is a crucial molecular event during M1 polarization, changes in this signaling definitely impair macrophages functioning as antigen presenting cells, and therefore hinder the initiation of adaptive immunity. A dramatic decrease of RT1-Ba (a MHCII molecular) was observed in XRF-ME treated CIA rats, which further confirmed the suppressive effects of xanthones on M1 polarization (Supplementary S9). Together with the evidences shown in Figure 2, we concluded that the inhibition of S-XANs on macrophages at least partially contributed to the eased CIA in rats.

Mounting evidences have confirmed the involvement of macrophages in metabolic disorders. Low-grade inflammation initiated by macrophages significantly contributes to obesity, diabetes and atherosclerosis.[27,28] At the same time, accelerated energy metabolism fuels inflammatory reactions.[27] Increased fat biosynthesis and utilization potently promote the development of RA, and the metabolic syndrome positively correlates to macrophages-related joints degradation.[18] Under such a background, the interplay between adipocytes and macrophages cannot be overlooked. As such, the disruption of metabolism-immunity feedback could serve as the foundation for pathological changes in RA. As revealed in Figure 6, the effects of both LPS and XAN on FLSs were amplified by the macrophage-pre-adipocytes co-culture system. It implies that aside from the direct inhibition on TLR4/NF-κB-controlled M1 polarization, XRF/XAN further reinforced the effects on the development of pro-inflammatory macrophages by targeting co-existing adipocytes.

As previously reported, *S. inappendiculata* have profound influences on energy metabolism. XRF obviously inhibited lipid anabolism in CIA rats.[8] Genome microarray analysis in this study further demonstrated that a panel of adipogenesis-related genes including Ces1d, Thrsp, Lpin2, SCD-1, Fasn, Tmem120b and Acvr1c were significantly down-regulated by XRF (Supplementary S9). More convincing evidence came from the metabolomic analysis (raw data were shown in Supplementary S10–S11). Treatment with XRF-ME caused significant decrease in the level of lipids in CIA rats (Figure 4). We also validated this phenomenon in experiments in vitro. XAN did not only inhibit the expression of mRNA SCD-1 and PPAR-γ in pre-adipocytes, but also substantially decreased the production of adiponectin (Figure 6). These metabolic changes would exert great impact on the internal environment. Firstly, the decreased lipid reserve could impair the defensive immune functions of macrophages because these ingredients are required for phagocytosis function and pro-inflammatory mediators synthesis.[29] Besides, the negative effects of XAN on adipogenesis could indirectly alter the polarization profile of macrophages. Suppressed adipogenesis is always accompanied with reduced circulating saturated FFAs, which possess the potentials of activating TLR4/NF-κB in macrophages.[16] Reduced adipokines have even more profound clinical implications. The pathological role of adipokines in RA and many other inflammatory-related diseases have been basically confirmed.[30] Although the mechanism through which adipokines reshape macrophages is not well understood, their impacts on immunity are huge.[31] Aside from the typical adipokines, many macrophages-related cytokines such as MCP-4 and MIP-1 are also defined as adipokines nowadays.[30,31] From this perspective, inhibiting the excretion of adipocytes is a feasible strategy to deal with macrophage-controlled inflammations in vivo. In this study, macrophages and pre-adipocytes were located in different chambers in transwell, and the pores between

them can only allow adipokines/cytokines and metabolites to permeate. Thus, the significant anti-inflammatory effects of XAN amplified in the co-culture system supported the claim above. Together, these evidences confirmed that XRF reinforced its anti-inflammatory effects by disrupting the interaction between macrophages and adipocytes.

Because XRF effectively altered lipid metabolism, it is not surprising to discover that it regulated PPAR-γ signaling in CIA rats.[21] In line with this, XAN reduced PPAR-γ expression in pre-adipocytes in vivo. It has the potential of inhibiting adipocytes differentiation, which consequently led to reduced adipokines production. Meanwhile, XAN promoted the expression of SIRT1 in pre-adipocytes, which plays an antagonistic metabolic role against PPAR-γ, and facilitates fatty acid oxidation.[20] Regulation of SIRT1 coordinated with PPAR-γ changes under XAN stimulus generally promoted fat catabolism, creating an environment favorable for M2 polarization.[32] On the contrary, XAN stimulus increased PPAR-γ expression in macrophages. It would further benefit the remission of local inflammation in joints, because PPAR-γ possesses notable anti-inflammatory trans-repression properties, and it is indispensable for IL4-mediated M2 polarization.[32] Unexpectedly, XAN inhibited SIRT1 expression in LPS-primed macrophages, which is a negative regulator of inflammation too.[33] It could be as a result of the SIRT1-PPAR-γ negative feedback.[20] But more plausibly, it was related to the alleviation of inflammations. SIRT1 instantly responds to NAMPT-provoked inflammation in order to quench the flame, and its necessity is not urgent anymore when the inflammation is resolved.[34] The opposite regulations of XRF/XAN on PPAR-γ signaling observed in macrophages and pre-adipocytes were indeed essential for the substantial improvement of immune milieu. However, the factor leading to diversified effects is still a puzzle yet to be resolved. It could be simply attributed to the different cell types. It could also be mediated by the immune changes. As shown in Figure 6A, LPS-primed macrophages were potent in increasing PPAR-γ in pre-adipocytes. Accordingly, impaired M1 polarization would decrease the effects of macrophages on PPAR-γ expression in targeted cells. More work is needed in order to validate these hypotheses. Although evidences from genome microarray analysis and in vitro assay suggested that XRF exerted varied effects on different types of cells, it generally up-regulated PPAR-γ signaling in joints in CIA rats, possibly because macrophages rather than pre-adipocytes are dominant PPAR-γ expressing cells there. Aside from related genes annotated by KEGG shown in Figure 3, PPAR-γ downstream Fgf1 and PPAR-γ positive regulator Senp2 were up-regulated, while the genes involved in negative regulation of PPAR-γ such as Acvr1c and Retn were down-regulated (Supplementary S9).

Conclusion

In this study, we revealed the joint protective effects of the bioactive fraction from *S. inappendiculata* in CIA rats over MTX. Aside from the effects on inflammatory pathways-controlled polarization of macrophages, XRF treatment brought profound impacts on immune microenvironment by regulating PPAR-γ signaling-controlled fat metabolism. Evidences from in vitro experiments further demonstrated that the representative *S. inappendiculata*-derived compound XAN can improve the immune milieu in joints by intervening into the metabolism-inflammation feedback, and consequently suppressed the erosive nature of FLSs acquired under inflammatory circumstances.

Abbreviations

RA, rheumatoid arthritis; CIA, collagen-induced arthritis; S-XANs, *S. inappendiculata*-derived xanthones; XAN, 1,7-dihydroxy-3,4-dimethoxyxanthone; XRF, xanthone-enriched fractions of *S. inappendiculata*; XRF-ME, XRF loading microemulsion; XRF-SU, XRF suspension.

Acknowledgments

This work was supported by National Natural Science Foundation of China (81973828, 81603388, and 81173596), Major Project of Natural Science Foundation of the Department of Education of Anhui province (KJ2020A0868, KJ2019ZD32), Funding of "Peak" Training Program for Scientific Research of Yijishan Hospital, Wannan Medical College (GF2019J01).

Disclosure

The authors report no conflicts of interest related to this work.

References

1. Zuo J, Xia Y, Li X, Chen JW. Therapeutic effects of dichloromethane fraction of *Securidaca inappendiculata* on adjuvant-induced arthritis in rat. *J Ethnopharmacol*. 2014;153(2):352–358.
2. Zuo J, Xia Y, Mao KJ, Li X, Chen JW. Xanthone-rich dichloromethane fraction of *Securidaca inappendiculata*, the possible antirheumatic material base with anti-inflammatory, analgesic, and immunodepressive effects. *Pharm Biol*. 2014;52(11):1367–1373. doi:10.3109/13880209.2014.892143

3. Zuo J, Mao KJ, Yuan F, Li X, Chen JW. Xanthones with anti-tumor activity isolated from *Securidaca inappendiculata*. *Med Chem Res*. 2014;23:4865–4871. doi:10.1007/s00044-014-1051-8
4. Zuo J, Xia Y, Li X, Li X, Chen JW. Xanthones from *Securidaca inappendiculata* exert significant therapeutic efficacy on adjuvant-induced arthritis in mice. *Inflammation*. 2014;37 (3):908–916. doi:10.1007/s10753-014-9810-8
5. Zuo J, Dou DY, Wang HF, Zhu YH, Li Y, Luan JJ. Reactive oxygen species mediated NF-κB/p38 feedback loop implicated in proliferation inhibition of HFLS-RA cells induced by 1,7-dihydroxy-3,4-dimethoxyxanthone. *Biomed Pharmacother*. 2017;94:1002–1009. doi:10.1016/j.biopha.2017.07.164
6. Ji CL, Jiang H, Tao MQ, Wu WT, Jiang J, Zuo J. Selective regulation of IKKβ/NF-κB pathway involved in proliferation inhibition of HFLS-RA cells induced by 1,7-dihydroxyl-3,4-dimethoxylxanthone. *Kaohsiung J Med Sci*. 2017;33(10):486–495. doi:10.1016/j.kjms.2017.06.015
7. Tao MQ, Ji CL, Wu YJ, et al. 1,7-Dihydroxy-3,4-dimethoxyxanthone inhibits lipopolysaccharide-induced inflammation in raw264.7 macrophages by suppressing TLR4/NF-κB signaling cascades. *Inflammation*. 2020;43(5):1821–1831. doi:10.1007/s10753-020-01256-3
8. Zuo J, Ji CL, Olatunji OJ, et al. Bioactive fractions from *Securidaca inappendiculata* alleviated collagen-induced arthritis in rats by regulating metabolism-related signaling. *Kaohsiung J Med Sci*. 2020;36 (7):523–534. doi:10.1002/kjm2.12205
9. Zuo J, Pan YL, Yuan F, Li X, Ju WZ. Quantitative determination of 2-hydroxy-1,7-dimethoxyxanthone in rat plasma by liquid chromatography-mass spectrometry. *Lat Am J Pharm*. 2014;33 (6):897–902.
10. Xu WK, Jiang H, Yang K, Wang YQ, Zhang Q, Zuo J. Development and in vivo evaluation of self-microemulsion as delivery system for α-mangostin. *Kaohsiung J Med Sci*. 2017;33(3):116–123. doi:10.1016/j.kjms.2016.12.003
11. Davignon JL, Hayder M, Baron M, et al. Targeting monocytes/macrophages in the treatment of rheumatoid arthritis. *Rheumatology*. 2013;52 (4):590–598. doi:10.1093/rheumatology/kes304
12. Neumann E, Lefèvre S, Zimmermann B, Gay S, Müller-Ladner U. Rheumatoid arthritis progression mediated by activated synovial fibroblasts. *Trends Mol Med*. 2010;16(10):458–468. doi:10.1016/j.molmed.2010.07.004
13. Wang DD, Li Y, Wu YJ, et al. Xanthones from *Securidaca inappendiculata* antagonized the antirheumatic effects of methotrexate in vivo by promoting its secretion into urine. *Expert Opin Drug Metab*. 2020:1–10. doi:10.1080/17425255.2021.1843634.
14. Cronstein BN. Low-dose methotrexate: a mainstay in the treatment of rheumatoid arthritis. *Pharmacol Rev*. 2005;57:163–172. doi:10.1124/pr.57.2.3
15. Harmon GS, Lam MT, Glass CK. PPARs and lipid ligands in inflammation and metabolism. *Chem Rev*. 2011;111(10):6321–6340. doi:10.1021/cr2001355
16. Rocha DM, Caldas AP, Oliveira LL, Bressan J, Hermsdorff HH. Saturated fatty acids trigger TLR4-mediated inflammatory response. *Atherosclerosis*. 2016;244:211–215. doi:10.1016/j.atherosclerosis.2015.11.015
17. Petkevicius K, Virtue S, Bidault G, et al. Accelerated phosphatidylcholine turnover in macrophages promotes adipose tissue inflammation in obesity. *eLife*. 2019. doi:10.7554/eLife.47990
18. Kerekes G, Nurmohamed MT, González-Gay MA, et al. Rheumatoid arthritis and metabolic syndrome. *Nat Rev Rheumatol*. 2014;10:691–696. doi:10.1038/nrrheum.2014.121
19. Larysa BB, Valentina MK. Pyrazinamide effects on cartilage type II collagen amino acid composition. *Int J Peptides*. 2012;2012:781785.
20. Han L, Zhou R, Niu J, McNutt MA, Wang P, Tong T. SIRT1 is regulated by a PPARγ-SIRT1 negative feedback loop associated with senescence. *Nucleic Acids Res*. 2010;38(21):7458–7471. doi:10.1093/nar/gkq609
21. Szanto A, Roszer T. Nuclear receptors in macrophages: a link between metabolism and inflammation. *FEBS Lett*. 2008;582 (1):106–116. doi:10.1016/j.febslet.2007.11.020
22. Gomes AS, Brandão P, Fernandes CSG, et al. Drug-like properties and ADME of xanthone derivatives: the antechamber of clinical trials. *Curr Med Chem*. 2016;23(32):3654–3686. doi:10.2174/0929867323666160425113058
23. Sharma AM, Staels B. Review: peroxisome proliferator-activated receptor gamma and adipose tissue–understanding obesity-related changes in regulation of lipid and glucose metabolism. *J Clin Endocr Metab*. 2007;92(2):386–395. doi:10.1210/jc.2006-1268
24. Zuo J, Qin Q, Wang L, et al. Mangosteen ethanol extract alleviated the severity of collagen-induced arthritis in rats and produced synergistic effects with methotrexate. *Pharm Biol*. 2018;56(1):455–464. doi:10.1080/13880209.2018.1506939
25. Yin Q, Wu YJ, Pan S, et al. Activation of cholinergic anti-inflammatory pathway in peripheral immune cells involved in therapeutic actions of α-mangostin on collagen induced arthritis in rats. *Drug Des Devel Ther*. 2020;14:1983–1993. doi:10.2147/DDDT.S249865
26. Zuo J, Yin Q, Wang YW, et al. Inhibition of NF-κB pathway in fibroblast-like synoviocytes by α-mangostin implicated in protective effects on joints in rats suffering from adjuvant-induced arthritis. *Int Immunopharmacol*. 2018;56:78–89. doi:10.1016/j.intimp.2018.01.016
27. Hotamisligil GS. Inflammation, metaflammation and immunometabolic disorders. *Nature*. 2017;542(7640):177–185. doi:10.1038/nature21363
28. Ye J, Keller JN. Regulation of energy metabolism by inflammation: a feedback response in obesity and calorie restriction. *Aging*. 2010;2 (6):361–368. doi:10.18632/aging.100155
29. Yan J, Horng T. Lipid metabolism in regulation of macrophage functions. *Trends Cell Biol*. 2020;30(12):979–989. doi:10.1016/j.tcb.2020.09.006
30. Hasseli R, Frommer KW, Schwarz M, et al. Adipokines and inflammation alter the interaction between rheumatoid arthritis synovial fibroblasts and endothelial cells. *Front Immunol*. 2020;11:925. doi:10.3389/fimmu.2020.00925
31. Lago F, Dieguez C, Gómez-Reino J, Gualillo O. Adipokines as emerging mediators of immune response and inflammation. *Nat Clin Pract Rheumatol*. 2007;3(12):716–724. doi:10.1038/ncprheum0674
32. Bouhlel MA, Derudas B, Rigamonti E, et al. PPARγ activation primes human monocytes into alternative M2 macrophages with anti-inflammatory properties. *Cell Metab*. 2007;6(2):137–143. doi:10.1016/j.cmet.2007.06.010
33. Kotas ME, Gorecki MC, Gillum MP. Sirtuin-1 is a nutrient-dependent modulator of inflammation. *Adipocyte*. 2013;2(2):113–118. doi:10.4161/adip.23437
34. Liu TF, Vachharajani VT, Yoza BK, McCall CE. Sirtuin 1 and 6 proteins coordinate a switch from glucose to fatty acid oxidation during the acute inflammatory response. *J Biol Chem*. 2012;287 (31):25758–25769. doi:10.1074/jbc.M112.362343